A study of ionopause perturbation and associated boundary wave formation at Venus

Ghai Siung Chong[1] ID **, Simon A. Pope[1] , Tielong Zhang[2,3]** ID **, Glyn A. Collinson[4]** ID **, Simon N. Walker[1] , and Michael A. Balikhin[1]**

[1] ACSE, University of Sheffield, Sheffield, UK, [2] Harbin Institute of Technology, Shenzhen, China, [3] Space Research Institute, Austrian Academy of Sciences, Graz, Austria, [4] Heliophysics Science Division, NASA Goddard Spaceflight Center, Greenbelt, Maryland, USA

Abstract Magnetometer and electron spectrometer data from Venus Express (VEX) are used to investigate the occurrence of boundary wave phenomenon occurring in the vicinity of the Venusian terminator. On 26 June 2006, VEX data show the ionosphere to be unmagnetized ($\approx$0 nT), a common observation usually expected during solar maximum. This results in the respective Venusian boundaries to be higher than the nominal altitudes. This paper reports the occurrence of rippling of the ionopause boundary in the terminator plane. The ripples appear to propagate mainly in the Y direction in the Venus solar orbital coordinates. Further examination of the first oscillation in magnetic field suggests that it is a flux rope. The flux rope is found to be just inside the ionosphere close to the ionopause. The diameters of the flux rope and boundary wave oscillations are estimated to be $\sim$113 km and $\sim$133 km, respectively. We suggest that the boundary wave is generated by the Kelvin-Helmholtz instability. This research provides evidence of the ionopause boundary existing in a wave-like state and its relation to Venus atmospheric loss into space.

1. Introduction

The study of the interaction of the solar wind with Venus is important for our understanding of the evolution of the atmosphere of Venus and other unmagnetized bodies in general. Earth and Venus, a pair of planets which are considered as twin sisters, are similar in many ways but yet also distinctly different. A recent 3-D climate simulation [*Way et al.*, 2016] has shown that Venus may have been a habitable planet millions of years ago, just like Earth today.

Previous studies have shown that Venus does not possess an intrinsic magnetic field [*Stevenson*, 2003; *Russell et al.*, 1980; *Stevenson et al.*, 1983; *Luhmann and Russell*, 1997]. For this reason, the solar wind interaction with Venus is comparably different to that with Earth which has a strong magnetic field. For instance, the Earth's magnetosphere is formed by the interaction of solar wind and the strong terrestrial magnetic field and has a stand off distance of $\sim$10 R_E (Earth radii) [*Sibeck et al.*, 1991]. In contrast, without an intrinsic magnetic field, the solar wind magnetic field piles up on the dayside ionosphere of Venus giving rise to an "induced magnetosphere" (also known as the "magnetic barrier"). The magnetopause is only around 1.05 R_V (Venus radius) at the subsolar point during solar minimum [*Zhang et al.*, 2008a].

Ever since in situ measurements of the Venusian ionosphere became available in the late seventies from the Pioneer Venus Orbiter (PVO), there have been plenty of studies documenting the observations of atmospheric plasma irregularities, for example, plasma clouds [*Brace et al.*, 1982]. These plasma clouds are irregularly shaped regions of ionospheric plasma that are detached from the ionosphere. They may correspond to a mechanism for atmospheric removal [*Brace et al.*, 1982]. They have previously been seen in observations and simulations in many locations such as the topside of the dayside ionosphere [*Brace et al.*, 1982], nightside ionosphere [*Brace et al.*, 1980], in the terminator plane [*Brace et al.*, 1980], magnetosheath [*Pope et al.*, 2009], and subsolar location (from simulation [*Terada et al.*, 2002]). All of these irregular plasma clouds have been argued to be evidence of the escape of the Venusian atmosphere into space.

The ionopause of Venus, which is a boundary that separates the planetary ionosphere from the shocked solar wind plasma, diverts the incoming solar wind to flow around Venus [*Theis et al.*, 1981; *Spreiter et al.*, 1970]. Large velocity shear between two different fluids can induce vortices and instability to the flow. In the case

Interior Structure of Flux Rope
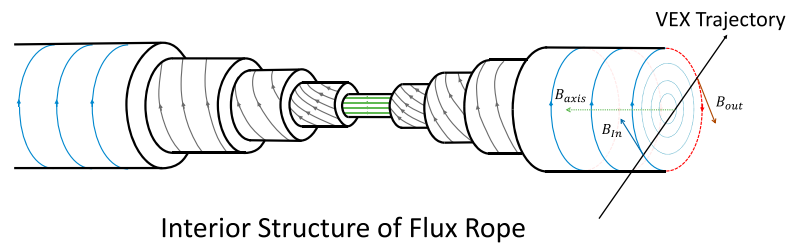
Figure 1. Illustration of the interior magnetic structure of a flux rope. (adapted from *Russell and Elphic* [1979]). The blue, green, and red arrows represent the magnetic field lines of the inbound boundary, central axis, and outbound boundary, and the grey arrows represent the magnetic field lines between the boundaries and the axis as well as the black straight arrow representing the trajectory of VEX.

of Venus, the observations of plasma and magnetic irregularities, e.g., flux ropes [*Wolff et al.*, 1980; *Russell et al.*, 1982; *Russell and Elphic*, 1979; *Elphic and Russell*, 1983] and "plasma clouds" (or "atmospheric bubbles") [*Wolff et al.*, 1980; *Brace et al.*, 1982; *Russell and Elphic*, 1979; *Russell et al.*, 1979], are closely associated with ionopause boundary waves, created by the solar wind flowing past the stationary ionosphere. The mechanism by which a boundary surface wave forms both detached plasma clouds and flux ropes is arguably the most effective atmospheric loss process at Venus [*Wolff et al.*, 1980; *Lammer et al.*, 2006; *Svedhem et al.*, 2007a; *Elphic et al.*, 1980]. Other atmospheric escape/erosion processes include photochemical reaction [*Lammer et al.*, 2006], thermal loss [*Lammer et al.*, 2006], photoion pickup, ionospheric holes [*Hartle and Grebowsky*, 1993], magnetotail magnetic reconnection [*Zhang et al.*, 2012], acceleration due to the $J \times B$ force, [*Dubinin et al.*, 2013] and solar wind pick up [*Lammer et al.*, 2006, and references therein].

There are two main potential instabilities for the generation of boundary waves at the Venusian ionopause, namely the interchange instability and Kelvin-Helmholtz Instability (KHI). The interchange instability only grows when there is a nonmonotonic plasma pressure gradient at the subsolar region [*Arshukova et al.*, 2004]. In contrast, KHI is an important mode of energy transfer and is considered the dominant instability. It can induce surface waves which can subsequently result in plasma loss [*Lammer et al.*, 2006; *Elphic and Ershkovich*, 1984; *Wolff et al.*, 1980; *Russell et al.*, 1979; *Russell and Elphic*, 1979; *Terada et al.*, 2002]. The tangential velocity shear flow, which is the strongest in the terminator region, is the primary seed for the development of the KHI [*Terada et al.*, 2002; *Amerstorfer et al.*, 2007; *Wolff et al.*, 1980; *Elphic and Ershkovich*, 1984; *Pope et al.*, 2009]. Other modes of excitation include velocity gradient [*Amerstorfer et al.*, 2007; *Ferrari et al.*, 1982; *Biernat et al.*, 2007; *Wolff et al.*, 1980] and other relatively weaker influences, i.e., density gradients [*Amerstorfer et al.*, 2007; *Huba*, 1981] and temperature gradients [*Huba*, 1981; *Price*, 2008].

When the rippling ionopause boundary reaches the final stage [*Fontane et al.*, 2008] of the KH wave, flux ropes, which are the current tubes containing shocked solar wind plasma, will detach from the main wave and scatter within the ionosphere and will eventually be convected downstream along the ionosheath flow [*Wolff et al.*, 1980]. In addition to the KHI, the observations of flux ropes within the ionosphere are also associated with mass loading [*Russell et al.*, 1982]. Mass loading occurs when the flux tubes, which normally lie on the dense ionospheric plasma, become heavier due to photoionization of neutral oxygen from the atmosphere and eventually sink into the ionosphere [*Russell*, 1990]. As they sink, the flux ropes will become more "twisted" and compressed within the atmospheric plasma. This gives them a three-dimensional helical structure [*Russell*, 1990]. An illustration of a flux rope is presented in Figure 1 (adapted from *Russell and Elphic* [1979]).

At the subsolar region, mass loading is a more favorable mechanism for flux rope generation (e.g., the observation in *Russell et al.* [1987]) in comparison to KHI because the shear flow is small. On the other hand, KHI is more favorable at the terminator region [*Terada et al.*, 2002] where the shear flow is greater. The magnetic features of these flux ropes were widely observed in the dayside ionosphere [*Elphic and Russell*, 1983] from PVO. From the ionopause, the occurrence of flux ropes increases with decreasing altitude, reaching a maximum at an altitude of around 165 km, before decreasing at lower altitudes. The diameters of the flux ropes are also dependent on the solar zenith angle (SZA). The diameters are smaller at the subsolar region (ranges from 6 to 12 km) and increase with increasing SZA, maximizing in the terminator region (ranges from 7.5 to 16 km) [*Elphic and Russell*, 1983; *Russell*, 1990]. The flux ropes are observed to be magnetically stronger (stronger magnetic field in the center) at around 165 km where their occurrences maximize and they are more tightly twisted at lower altitude and lower SZA [*Elphic and Russell*, 1983]. The "twist" is measured by the degree

of flux rope helicity. In minimum variance (MV) analysis, the twist is measured by the angle of the hodogram as it approaches the origin in the maximum variance [*Russell*, 1990]. More detailed information on the measure of the helicity can be found in *Elphic and Russell* [1983].

In this paper, evidence of boundary waves observed by VEX on 26 June 2006 is presented. We investigate the evolution of these boundary waves in the terminator region of the ionopause by examining a sequence of magnetic oscillations. On 26 June 2006, within the boundary, evidence is shown for the existence of a magnetic flux rope. The observation of boundary waves in this study is fundamental in explaining the observations of ionospheric plasma-like structures outside the ionosphere [*Brace et al.*, 1980, 1982]. Finally, we discuss their dynamics and show that their properties are consistent with a previously proposed generation mechanism which may contribute to Venusian atmospheric evolution.

2. Instrumentation
2.1. Venus Express
VEX was in an elliptical polar orbit with apoapsis distance of 66,000 km and a period of 24 h. The periapsis ranged from 250 to 350 km and was at a latitude of about 78°N [*Titov et al.*, 2006; *Svedhem et al.*, 2007b]. The magnetic field was measured by the VEX fluxgate magnetometer [*Zhang et al.*, 2006]. The sampling mode was changed depending on orbital position. The normal sampling mode was 1 Hz, with 32 Hz mode for an hour either side of periapsis and 128 Hz for 2 min at periapsis. The instrument had two sensors enabling the removal of stray fields due to the magnetically dirty spacecraft [*Pope et al.*, 2011]. The 32 Hz MAG data are used in this paper for higher-resolution analysis. The data have been rotated into Venus Solar Orbital (VSO) coordinates; with X_{VSO} in the Venus-Sun direction, Y_{VSO} is in the direction of the orbital motion of Venus and Z_{VSO} completes the right hand upward out of the ecliptic orbital plane. The Analyzer of Space Plasmas and Energetic Atoms (ASPERA-4) on board VEX included four sensors; electron spectrometer (ELS), ion mass analyzer (IMA), neutral particle imager (NPI), and neutral particle detector (NPD) [*Barabash et al.*, 2007]. Only ELS data are used in this paper. The ELS, which had 16 sectors of 22.5° covering the full 360° cycle with a resolution of 32 s, measured the energy spectrum of the electron populations.

3. Data Analysis
The trajectory of VEX on 26 June 2006 and the nominal position of the bow shock (blue), the induced magnetopause (red), and the ionosphere (green) are shown in Figure 2. On this day, VEX was traveling almost along the terminator with SZA ranging from 84° (inbound shock crossing at 01:29:51 UT) to 95° (outbound shock crossing at 02:30:32 UT). Orbits in the vicinity of the terminator provide an ideal opportunity to study fluctuations of the ionopause boundary because it gives a higher probability of encountering the boundary wave (if the boundary is indeed fluctuating) in comparison to the orbits along the Sun-Venus line. The magnetic field and electron energy spectrum are shown in Figures 3a and 3b, respectively. The magnetic field magnitude plot in Figure 3a is divided into six different regions labeled in upper case Roman numerals. VEX can be seen crossing the bow shock at 01:29:51 UT (at an altitude of about 4387 km). There are some notable oscillations (Region I) prior crossing the bow shock on 26 June 2006. The shock angle θ_{Bn} is ≈30°, based on an average value obtained using minimum variance (MV) analysis (32°) [*Sonnerup and Scheible*, 1998; *Sonnerup and Cahill*, 1968], coplanarity (34°) [*Schwartz*, 1998, and references therein], and model Bow shock (24°) [*Zhang et al.*, 2008b]. These structures could be attributed to either foreshock magnetic structures (e.g., Short Large Amplitude Magnetic Structures (SLAMS) [*Collinson et al.*, 2012]) or multiple shocks crossings. Such magnetic oscillations are quite common for quasi-parallel shocks. As the spacecraft crossed the bow shock into the magnetosheath (Region II), the incoming solar wind electrons are heated by the shock, broadening the electron energy distribution. The broad energy intensity (ranging from ~11 eV to ~70 eV) in this region is maintained until 01:42:42 UT where the energy distribution can be seen to become narrower toward the lower boundary of the magnetosheath. At around 01:43:08 UT, VEX crosses the magnetopause and enters the magnetic barrier (Region III), which may be described as the "transition layer" [*Coates et al.*, 2008]. In the magnetic barrier, the electron distribution broadens, spanning 3 eV to 70 eV which shows a mixture of sheath-like (~11 eV to 70 eV) and ionospheric (3 eV to ~11 eV) plasma. The lower boundary of the magnetic barrier is not particularly obvious here; the electron distribution remains broad without an obvious peak until 01:45:55 UT (altitude of 768 km). The ionospheric plasma (Region IV) is characterized by a narrow peak that intensifies at around 18 eV, while there are some pulse-like dropouts from 01:47:14 (altitude of 600 km) to 01:51:00 UT (altitude of 323 km). Ionospheric plasma was constantly observed by VEX until 01:59:07 UT
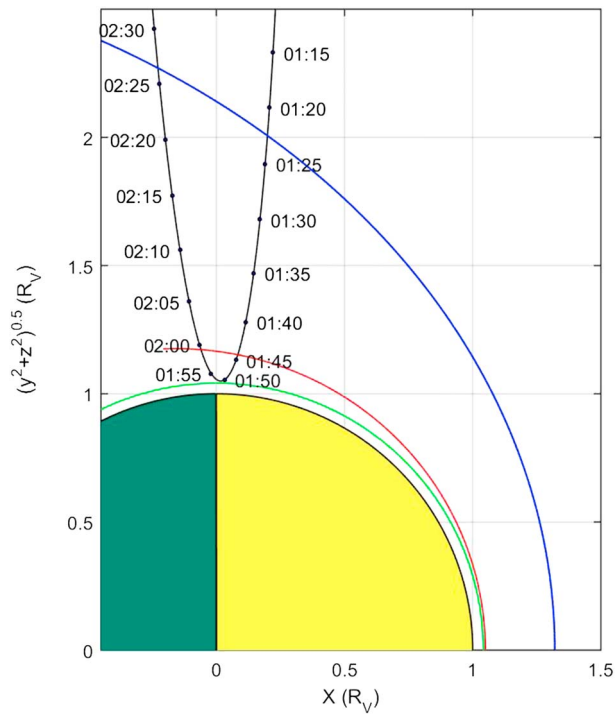
Figure 2. The trajectory of Venus Express (black) on 26 June 2006 and the nominal position of the bow shock (blue) [*Zhang et al.*, 2008b], induced magnetopause (red) [*Zhang et al.*, 2008a], and the ionosphere (green) [*Zhang et al.*, 2008a]. The dayside and nightside of Venus surface are shaded in yellow and dark green. The orbit is also labeled with UT in black colored dots.

VEX data on 2006-06-26
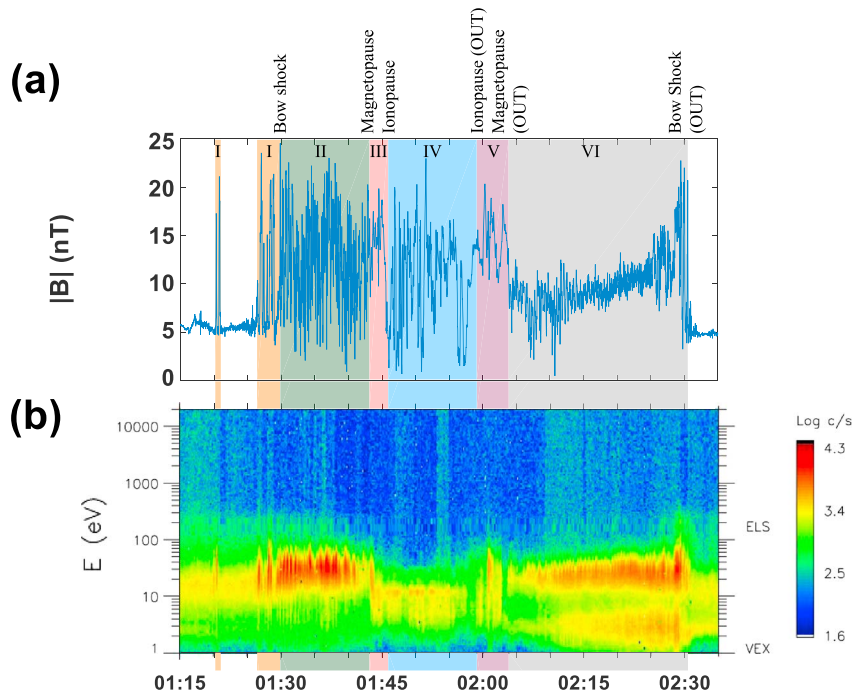
Figure 3. VEX magnetic field and electron energy distribution measurements from 01:15 to 02:35 UT on 26 June 2006. (a) Magnitude of the magnetic field. The plot is shaded to highlight six different regions; Region I represents the upstream oscillations regions, Region II the magnetosheath, Region III the magnetic barrier, Region IV the region in which ionospheric plasma is detected, Region V the outbound magnetic barrier, and Region VI the outbound magnetosheath. (b) Energy-time spectrogram of electron count rate.
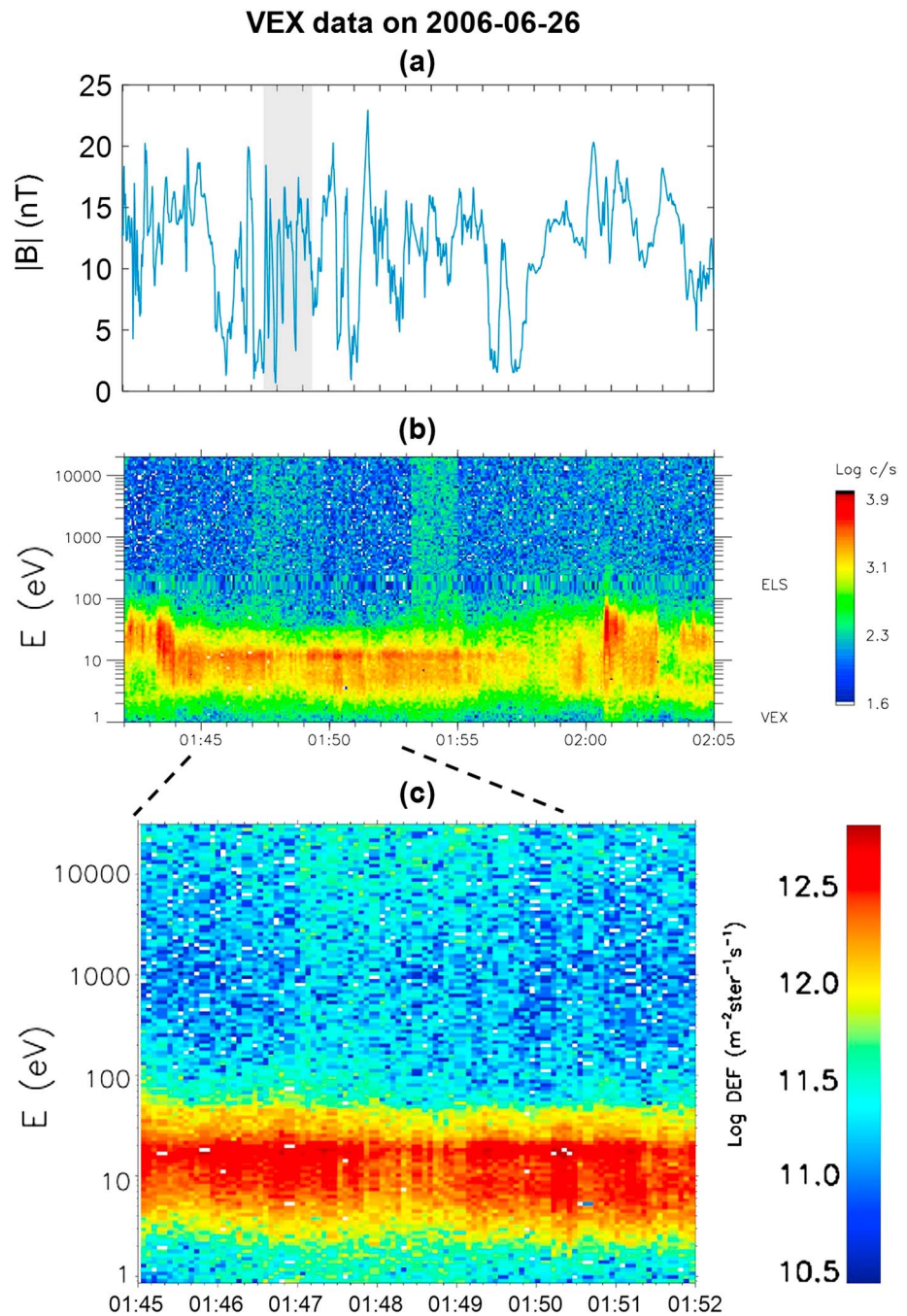
Figure 4. (a) Magnitude of the magnetic field, (b) energy-time spectrogram of electron count rate from 01:42 to 02:05 UT on 26 June 2006, and (c) a section of the energy-time spectrogram from 01:45 to 01:52 UT which shows multiple pulse-like dropouts in the electron count rate.

when the spacecraft traveled into the outbound magnetic barrier (Region V). Similar to the inbound region, VEX detected a mixture of sheath-like and ionospheric plasma populations in the outbound magnetic barrier, as evidenced from the electron spectrogram; the broad electron distribution spans from 3 eV to 70 eV. The spacecraft then crossed the magnetopause at 02:03:52 UT into the outbound magnetosheath (Region VI) and eventually crossed the bow shock again at 02:30:32 UT.

3.1. Observation of the Boundary Wave

Figure 4 shows the magnetic field and electron energy spectrum measured within the ionosphere (Region IV of Figure 3) in greater detail. From Figure 4a, it is clearly seen that the magnetic field drops almost to 0 nT
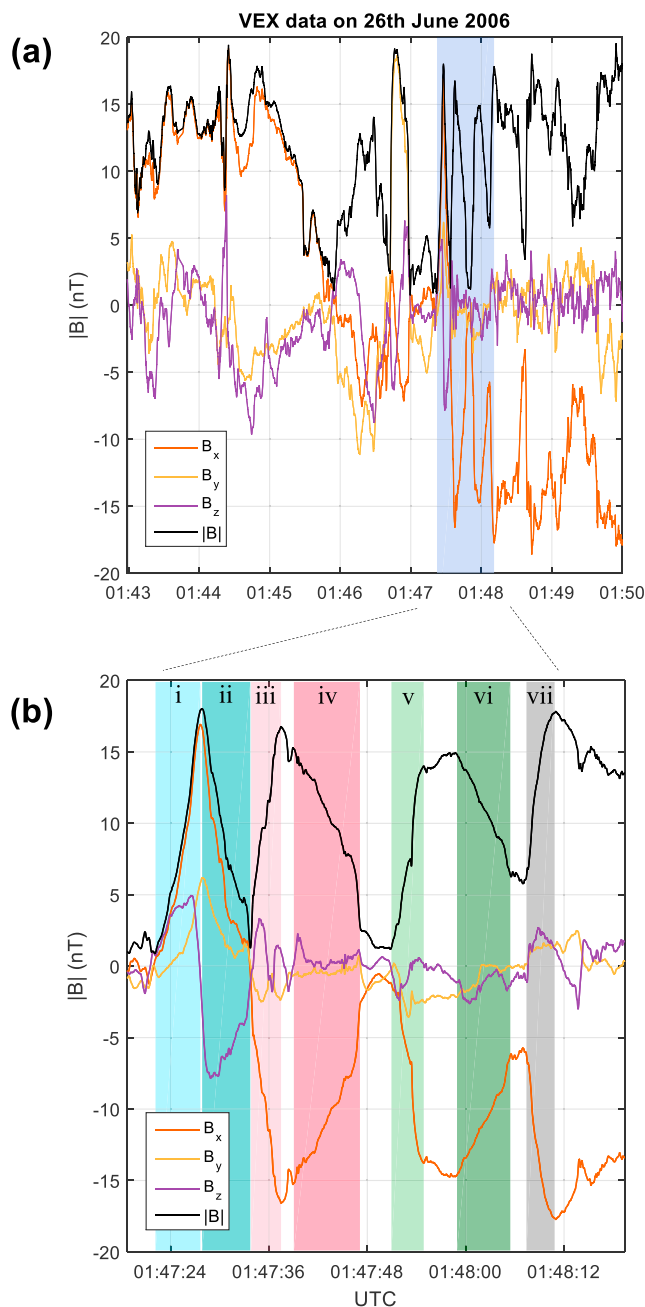
Figure 5. (a) A section of the Venus Express data on the 26 June 2006 which shows the magnetic field components from 01:43 to 01:50 UT. The blue-shaded region is enlarged and is shown in Figure 5b. (b) A section of the Venus Express data on the 26 June 2006 which shows seven consecutive oscillations (dip-to-peak and peak-to-dip) of the magnetic field. The black plot represents the field magnitude, the red, yellow, and purple represent the field components in X, Y, and Z directions, respectively. Each dip-to-peak-to-dip is also shaded in lighter and darker shade of colors for ease of identification.

on a number of occasions, e.g., 01:46:02, 01:47:07, 01:47:30, 01:47:57, and 01:50:54 UT. These dips of the field correspond to pulse-like dropouts in the electron energy spectrogram which indicates that VEX repeatedly traverses the ionopause a numerous time, passing from high field sheath to low field ionosphere (clearly shown in the grey-shaded region in Figure 4) which may indicate a boundary wave. Figure 5b shows the magnetic field data (in X, Y, and Z directions) over a section of this consecutive oscillations region (01:47:22 to 01:48:12 UT). The field magnitude shows three distinct oscillations between sheath and ionospheric levels, with the magnetic field data oscillating from around 2 nT to 18 nT. These dip-to-peak and peak-to-dip

Table 1. A Summary of the Results of the Minimum Variance Analysis on Venus Express Data on 26 June 2006 for All the Intervals "01:47:22–01:47:28", "01:47:34–01:47:38", "01:47:51–01:47:55", "01:48:08–01:48:11", "01:47:28–01:47:34", "01:47:40–01:47:48", and "01:47:59–01:48:06"

Time (UTS)		MV Direction			Eigenvalues			$\lambda2/\lambda1$	$\lambda3/\lambda2$	B_n (nT)	$|B_n|/|B|$	$\theta_{B_n\_B}$, (deg)	θ_{VEX_MV}, (deg)
From	To	X	Y	Z	$\lambda1$	$\lambda2$	$\lambda3$						
					Dips to Peaks								
01:47:22	01:47:28	−0.33	0.92	0.23	0.038	3.078	33.125	81.28	10.76	−0.33	0.04	87.63	16.34
01:47:34	01:47:38	−0.06	0.92	0.39	0.016	2.610	19.148	159.98	7.34	−0.44	0.04	87.55	18.88
01:47:51	01:47:55	0.19	−0.15	0.97	0.281	0.743	20.721	2.64	27.91	−1.62	0.22	77.43	85.25
01:48:08	01:48:11	0.05	0.97	−0.24	0.017	0.565	16.983	32.32	30.08	0.06	0.00	89.76	16.27
					Peaks to Dips								
01:47:28	01:47:34	0.36	−0.93	0.10	0.091	2.038	26.096	22.36	12.81	−0.56	0.06	86.52	159.44
01:47:40	01:47:48	0.07	−1.00	0.03	0.042	0.213	8.794	5.10	41.30	0.40	0.04	87.76	172.85
01:47:59	01:48:06	0.19	−0.87	0.45	0.114	0.419	6.007	3.68	14.35	−2.08	0.19	79.40	148.87

magnetic field correspond to the pulse-like dropouts in the electron energy spectrogram, visible from Figure 4c. Each of the dip-to-peak and peak-to-dip is shaded in different colors and is labeled in lower case Roman numerals for ease of identification. Table 1 shows the minimum variance [*Sonnerup and Scheible*, 1998] components in the X, Y, and Z directions, the eigenvalues (λ_1, λ_2, λ_3), intermediate-to-minimum eigenvalues ratio (λ_2/λ_1), the maximum-to-intermediate eigenvalues ratio (λ_3/λ_2), the average magnetic field component along the minimum variance direction (B_n), the ratio of B_n to the total magnetic field magnitude ($|B_n|/|B|$), the angle between $|B_n|$ and $|B|$, $\theta_{B_n\_B}$, and the angle between the spacecraft trajectory and the minimum variance directions, θ_{VEX_MV}. To check the consistency of the results, each of the dip-to-peak and peak-to-dip is divided into several segments and is further analyzed (the details are attached in Table S1 in the supporting information).
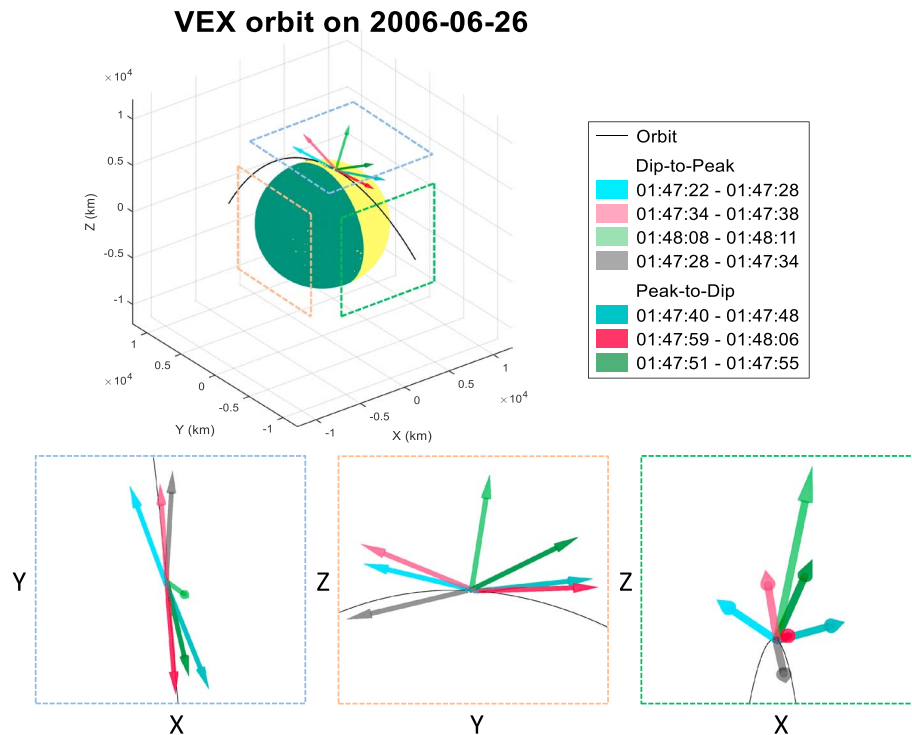
Figure 6. Three-dimensional views of minimum variance directions of all the seven "peak-to-dip" and "dip-to-peak" intervals on 26 June 2006. The intervals "01:47:22–01:47:28", "01:47:34–01:47:38", "01:47:51–01:47:55", "01:48:08–01:48:11", "01:47:28–01:47:34", "01:47:40–01:47:48", and "01:47:59–01:48:06" are color labeled with respect to their minimum variance directions. The color-dotted frames are 2-D views of the trajectory where pink is X-Z plane, green is Y-Z plane, and blue is X-Y plane.

(a)

(b)
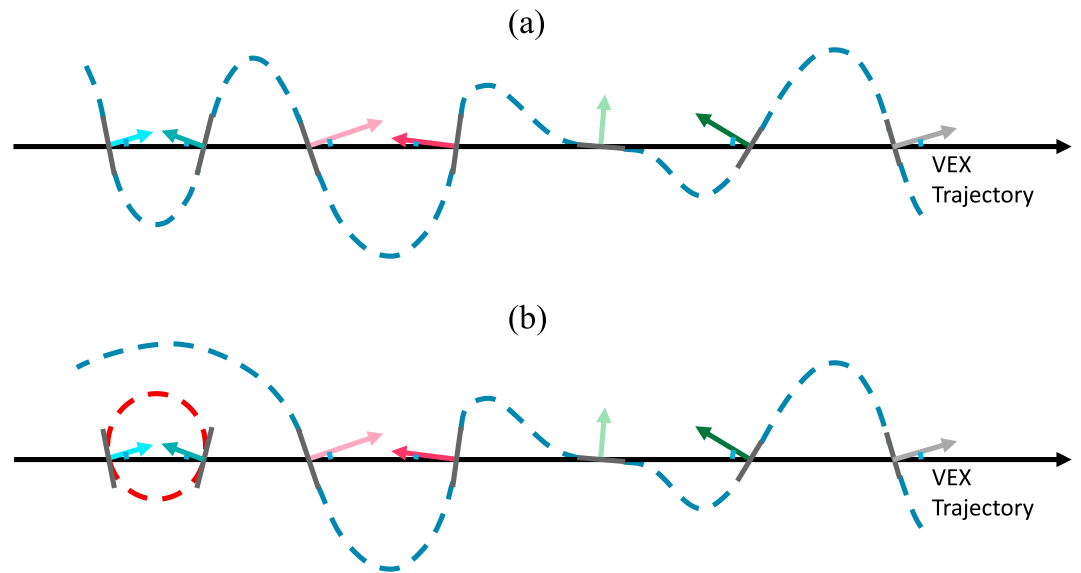
Figure 7. (a) An illustration of the boundary wave observed from 01:47:22 to 01:48:12 UT. The normal directions of the boundaries are represented by the arrows. The arrows are color coded according to Table 1. The grey lines represent the instantaneous boundaries which VEX crosses. The blue dotted line completed the illustrative shapes of the boundaries. The black straight arrow represents the trajectory of VEX. (b) A similar illustration of the boundary wave, but also including an isolated flux rope represented as a red dotted line.

The minimum variance directions of all seven intervals for the periods corresponding to successive dip-to-peak and peak-to-dip magnetic oscillations are plotted against the orbit in Figure 6; both the figure and the table are color coded. The minimum variance directions for the dip-to-peak intervals are very well defined with intermediate-to-minimum eigenvalues (λ_2/λ_1) > 32, apart from Region v (01:47:51 to 01:47:55 UT) which the minimum variance direction is less well defined (λ_2/λ_1 of 2.64). This may be affected by the magnetic field intermediary at 01:47:54 UT (center of Region v). The minimum variance directions for the peak-to-dip intervals are also less well defined with λ_2/λ_1 > 3.68.

It is noticeable from Figures 5a and 5b that the main changes of the field measurement in this period are mostly in the X direction. Apart from Regions i and ii, the Y and Z components are relatively close to zero (~±3 nT). The average total magnetic field dips in this duration are also close to 0 nT (~2 nT) which may indicate VEX was traveling in the ionosphere region where the plasma is almost unmagnetized. Additionally, all seven of the B_n components are small compared to their respective mean field magnitudes $|B_n|/|B| < 0.22$ and are well lower than the upper boundary of a tangential discontinuity ($|B_n|/|B| < 0.3$) [*Lepping and Behannon*, 1980] indicating that this boundary represents a tangential discontinuity (a discontinuity that is characterized by zero normal mass flow [*Baumjohann et al.*, 1996]). The tendency of the angle between $|B_n|$ and $|B|$ to be 90° (all angles are >77.4°) further indicates that this is a tangential discontinuity, a typical characteristic of the Venusian ionopause [*Wolff et al.*, 1980].

The angle between the trajectory of VEX and the minimum variance directions from each of the dip-to-peak and peak-to-dip transition is shown in Table 1. All seven angles with respect to the VEX trajectory (plotted as a black straight horizontal arrow) are shown in Figure 7a. The seven arrows, which are color coded with their respective intervals in Table 1, represent the minimum variance direction of each of the seven boundary crossings. The bold grey lines, which form a perpendicular plane to the minimum variance directions, represent the instantaneous boundaries crossed by VEX. An illustrative shape of the potential boundary is traced with the blue dotted line. The observed changes in angles between the VEX trajectory and the boundary normals indicate the existence of a boundary wave, e.g., Figure 7a. Even though the angles θ_{VEX_MV} were taken into consideration when plotting this figure, the shape and structure only serve as an illustrative example. Furthermore, as shown in Figure 6, the minimum variance directions of the dip-to-peak field tend to be directed in the negative Y direction while the minimum variance directions of the peak-to-dip intervals are directed in the positive Y direction; this (as shown in Figure 7a) suggests that VEX traversed through the ionopause boundary which propagates in the Y direction numerous times.
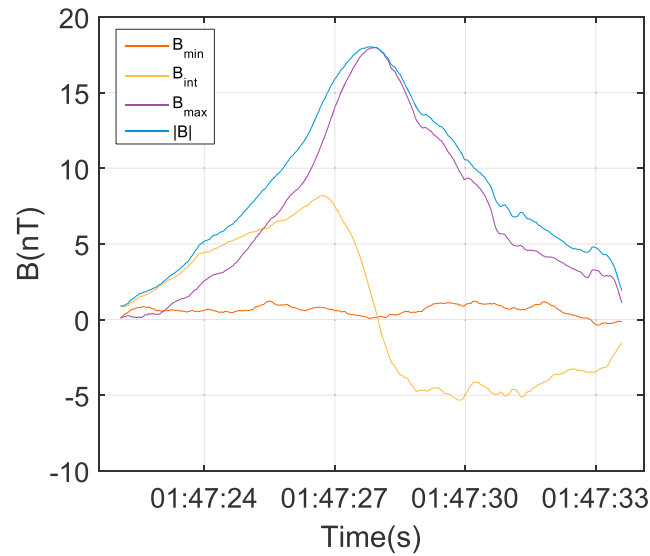
Figure 8. The magnetic field (minimum, intermediate, and maximum variance directions) of the observed flux rope.

3.2. Observation of a Flux Rope

While most of the magnetic wave trains from the previous section (01:47:22 to 01:48:12 UT in Figure 5b) show properties of a two-dimensional planar magnetic structure, the first dip-to-peak-to-dip from 01:47:23 to 01:47:34 UT (Regions i and ii) shows a three-dimensional magnetic structure that has a close resemblance to those of a flux rope. This flux rope is observed at an altitude of 574 km and SZA of 87°. The minimum B_{min}, intermediate B_{int}, and maximum B_{max} variance components of its magnetic field are shown in Figure 8.

From Figure 8, the magnetic field strength is observed to be the lowest ($\sim$1 nT) at the boundaries of the magnetic structure (corresponds to the begin and the end of the field magnitude plot). The magnetic field strength increases as the structure is crossed gradually, peaking in the maximum variance direction ($\sim$18 nT) before it decreases toward the exiting boundary. In addition, it is seen in Figure 8 that when the magnetic field in the maximum variance direction B_{max} is at its peak strength, the intermediate and minimum variance components B_{int} and B_{min} reach minimum ($\approx$ 0nT). This suggests that VEX crosses a magnetic structure with weak field strength at the boundaries and strong axial field in its center, e.g., a flux rope. Note that unless the spacecraft passes through the exact center of the flux rope, there will be a finite azimuthal field component perpendicular to its axis.

To find out if these changes of direction are three-dimensional, further analysis is conducted. Figure 1 shows the magnetic structure of a flux rope (adapted from *Russell and Elphic* [1979]). The blue, green, and red arrows (labeled B_{in}, B_{axis}, and B_{out}) that represent the instantaneous magnetic field directions which VEX crosses at the inbound boundary, central axis, and outbound boundary. If the VEX trajectory is assumed to cross the flux rope as illustrated in Figure 1, and if the direction of the peak magnetic field is assumed in the direction of the axis (B_{axis}) of the flux rope, the angle between the field direction at the inbound crossing of the boundary (B_{in}) and the axis (B_{axis}) from the analysis is found to be 77°. Similarly, the angle between the field direction at the outbound crossing of the boundary (B_{out}) and axis (B_{axis}) is 54°. The existence of these rotations between B_{in}, B_{axis}, and B_{out} shows that the field rotation is three dimensional as illustrated in Figure 1, implying that the structure which VEX traversed through is not just a two-dimensional planar magnetic structure. All the above observations are consistent with the signature characteristics of a flux rope.

Furthermore, while the minimum variance component B_{min} (orange) is close to 0 nT throughout the interval, it is visible from Figure 8 that the direction of the intermediate variance component B_{int} (yellow) flips 180° quickly (in just under 2 s) as the maximum variance component B_{max} (purple) reaches its maxima. This observation is consistent with the typical characteristic of the structure of a flux rope. If B_{int} represents B_{in} in Figure 1, B_{int} decreases as VEX passes through the flux rope and it will reach minima (zero in our case) when VEX passes through/close to the center of the flux rope (as the main magnetic field component will be along the axis).
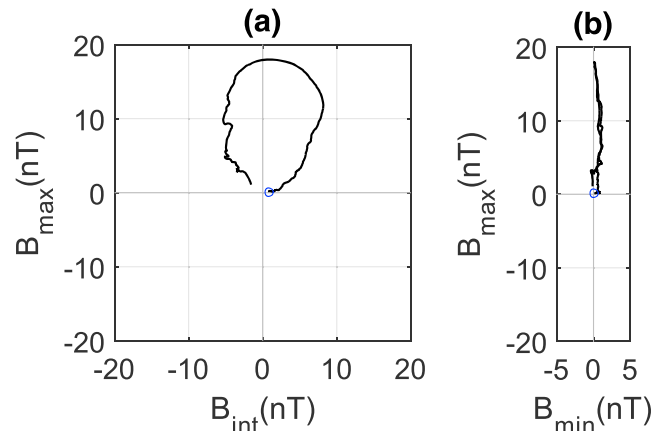
Figure 9. (a) Hodogram of the field variation in B_{max} to B_{int} plane. (b) The width of the flux rope in B_{max} to B_{min} plane from 01:47:23 to 01:47:34 UT.

Similarly, as VEX leaves the center of the flux rope, B_{int} increases but in the opposite direction and eventually reaches B_{out} when VEX traversed through the outbound boundary, i.e., the B_{in} and B_{out} are 180° opposite in direction.

The hodogram of the variance components is shown in Figures 9a and 9b. The start of the hodogram plot is marked with a blue circle. The minimum variance direction of this magnetic structure is very well defined with eigenvalues ratio of $\lambda_2/\lambda_1 > 169$. It can be seen that the magnetic field direction rotates by 180° as VEX traverses through the magnetic structure which is consistent with our observation from Figure 8a.

Another key identifier that this magnetic structure is in fact a flux rope and not some planar magnetic structures is the "potato chip" shape hodogram [*Russell*, 1990] as shown in Figure 9b that indicates the magnetic structure is axially twisted. In comparison to this potato chip shape, a vertical line of B_{max}/B_{min} would have indicated that the magnetic structure is "untwisted", i.e., not a flux rope.

In comparison to Figure 7a, the observation of a flux rope and how it may exist within the boundary wave is illustrated in Figure 7b. Both of the plots only serve as an illustration. Due to the limitations of Venus Express instrumentation and without further analysis, the exact physical structure of the flux rope and the boundary wave cannot be determined with certainty.

Another stronger flux rope ($|B| \approx 43$ nT) has also been observed on 20 June 2006. During this observation the ionosphere was again unmagnetized. The results from the data analysis of both 20 June 2006 and 26 June 2006 are very similar (the results of the minimum variance analysis of this flux rope are attached in Table S2, Figures S1, and S2 in the supporting information). The flux rope was observed at 612 km and a SZA of 97°. The $\lambda_2/\lambda_1 = 51$ and $B_n \approx 0$ show a very well-defined boundary with a tangential discontinuity. However, the hodogram is not as twisted compared to 26 June 2006.

4. Discussion

This paper has presented the results of the observation of boundary waves and a flux rope on the 26 June 2006 using the VEX magnetic field and plasma measurement data.

4.1. Altitude of the Ionopause

Even though the plasma data measured from the ELS as well as the MV parameters from the data analysis are consistent with the signatures of the Venusian ionopause, the altitude at which the boundary wave and flux rope are observed on 26 June 2006 is much higher than the nominal altitude of the ionopause during solar minimum (572 km compared to the nominal 250 km *Zhang et al.* [2008a]). Furthermore, during solar minimum, the ionosphere is expected to be magnetized most of the time [*Zhang et al.*, 2007], a state which often contains large-scale magnetic field structures. Since such field structures may suppress the formation and the observation of flux ropes, flux ropes are infrequently observed even though they are observed more than 70% of the orbits of PVO (during solar maximum) [*Elphic and Russell*, 1983].

Although it may not be a common observation, the terminator ionopause has previously been observed at much higher altitudes (>700 km) during solar minimum [*Zhang et al.*, 2008a; *Coates et al.*, 2008; *Futaana et al.*, 2008] and has been observed as high as 900 km during solar maximum [*Zhang et al.*, 2008a]. The Venus ionosphere can also sometimes be observed field free at solar minimum (an unmagnetized ionosphere was observed in 39 out of 225 VEX orbits from 24 April to 30 December in 2006 according to *Wei et al.* [2010]) and resemble the environment at solar maximum; e.g., on 26 June 2006 when the magnetic field strength |*B*| of the ionosphere is ≈0 nT. The preliminary survey of VEX in 2006 by *Zhang et al.* [2008a] shows that about 5% of the orbits are unmagnetized, of which are all under extreme solar conditions, e.g., interplanetary coronal mass ejection (ICME) events [*Futaana et al.*, 2008] and interplanetary magnetic field (IMF) alignment with solar wind flow [*Zhang et al.*, 2009]. Further analysis of the VEX magnetic field data in a period of ±15 days of this date shows a mixture of magnetized and unmagnetized ionosphere, with a higher occurrence of the former.

Although the periapsis of VEX is consistently around 250–350 km and because the nominal altitude of the Venusian ionopause is 250 km [*Zhang et al.*, 2008a], VEX normally only crosses the ionopause for a very short time (or not at all) during solar minimum. This could also explain why physical boundary waves are rarely observed during solar minimum. In addition, significant disturbance of the ionopause boundary due to the waves may also result in crossings being observed at higher than expected altitudes.

4.2. Kelvin-Helmholtz Instability and the Paucity of the Observations

The flux rope and boundary wave are observed close to the terminator (SZA of 86.8°). The strong velocity shear in the terminator region is a principal seed excitation for the development of the KHI [*Terada et al.*, 2002; *Amerstorfer et al.*, 2007; *Wolff et al.*, 1980; *Elphic and Ershkovich*, 1984; *Pope et al.*, 2009; *Pérez-de Tejada et al.*, 1977]. As the boundary wave grows and develops from the linear to nonlinear regime, vortices can form. These vortices can roll up and eventually break up forming bubbles of ionospheric plasma. These detached ionospheric bubbles are eventually convected downstream by the magnetosheath flow. This process is subsequently responsible for atmospheric plasma loss of Venus [*Lammer et al.*, 2006; *Elphic and Ershkovich*, 1984; *Wolff et al.*, 1980; *Brace et al.*, 1982; *Russell et al.*, 1979; *Russell and Elphic*, 1979; *Terada et al.*, 2002]. Over the period where the rippling ionopause boundary is observed (01:47:22 to 01:48:12 UT), the approximately perpendicular orientation between the magnetic field direction in the magnetic barrier region (mainly in *X* direction) and the wave normal of the ionopause boundary (which are represented by the minimum variance directions which are mainly in *Y* direction) also contributes to the stability condition of the KHI [*Wolff et al.*, 1980].

Flux ropes can be produced in the subsolar region by the mass loading process and may be transported into the nightside through the terminator region. Although the periapsis of VEX was maintained at around 250 km (nominal ionopause altitude), the population of flux ropes has been shown to be greatest at lower altitudes (highest population is around 165 km according to *Russell and Elphic* [1979] and *Elphic and Russell* [1983]); therefore VEX observations of flux ropes tend to be infrequent. On the other hand, atmospheric bubbles and flux ropes are both produced in the terminator region [*Brace et al.*, 1982] and can coexist in theory. However, by the time the atmospheric bubbles are fully developed, they have already been transported downstream into the nightside. This can explain the paucity of the observations of the atmospheric bubbles in the dayside. In addition, there are only an estimated 12 plasma clouds in the cloud zone at any time [*Brace et al.*, 1982].

4.3. Shape and Sizes

If the assumption is made that VEX is traveling perpendicularly into a stationary flux rope, the average width of each oscillation and the flux rope is ∼133 km and ∼113 km, respectively. This is estimated from the average speed of VEX (9.5 km s^{-1}) and time spent during the crossing. If the flux rope is assumed to be moving at the local Alfven speed, ±1 km s^{-1} [*Elphic and Russell*, 1983] or less (relative to VEX trajectory), then the width of the flux rope would be ∼101 or ∼125 km. Finally, on the assumption that the wave is traveling parallel to the surface of Venus, which at the terminator is in the *y-z* plane, the projection of the minimum variance direction determined from the boundary crossing can be used as an estimate of the direction of propagation of the wave. On this assumption the widths of the flux rope are ∼104 or ∼128 km. The observations discussed in this paper suggest that the structure has the characteristics of a flux rope. However, the estimated width is significantly greater than the upper boundary of the estimated diameter (16 km in the terminator region) suggested by *Russell* [1990]. One explanation for this is that the flux rope is newly created before the center line of the draping. It is then observed just underneath the ionopause after VEX crosses the center line of the draping (this is discussed further in section 4.4). Flux ropes become more twisted as they travel deeper into
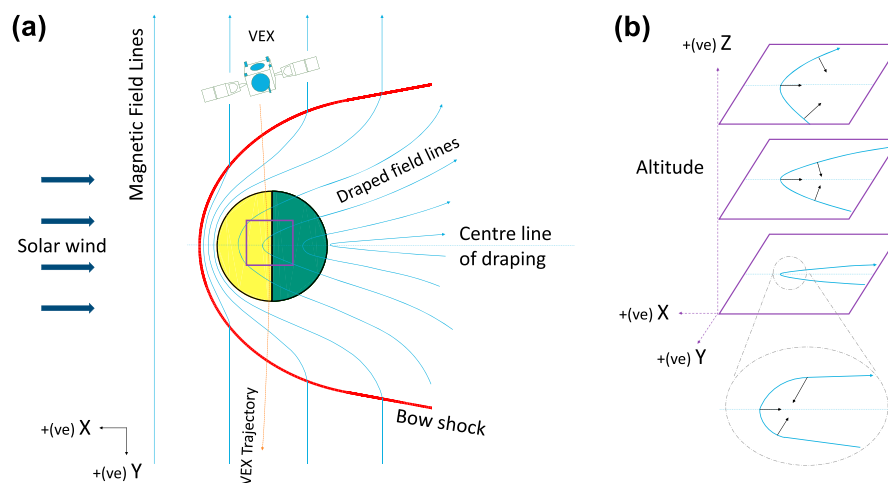
Figure 10. (a) Illustration of field draping around Venus in the *X-Y* plane. The magnetic field lines are represented by the blue arrows. As they are swept toward the planet, they start to drape around the planet with the field lines extending in the −*X* direction. (b) Illustrates the change in field line draping as a function of altitude for the area in the purple square box. The black arrows represent the normals to the field line directions as they drape around the planet. As the altitude decreases the directions of the field lines become more antiparallel along the flanks of the draping.

the ionosphere, resulting in a decrease in their width. This can be attributed to the Helical Kink Instability [*Russell*, 1990]. Furthermore, based on the plasma parameters obtained from PVO, *Wolff et al.* [1980] show that the wavelengths of the KHI can range from around 50 km to 150 km. Since the flux rope is observed very close to the ionopause boundary and the estimated width of the flux rope of around 113 km is in the range of the KHI wavelength in *Wolff et al.* [1980], hence the estimated width is within the possible limit.

Since only one flux rope is observed in our study, in comparison to *Elphic and Russell* [1983] which includes statistical variations, our estimation of its width depends on how the spacecraft encounters the flux rope. For example, different width calculations will result if VEX traverses through the exact center of the axis or just off center. In addition, flux ropes can diffuse within the ionosphere and exist in an elongated shape in the ionosphere [*Wolff et al.*, 1980]. This could create marginal variations in the calculation. Furthermore, the magnetic field lines are draped as illustrated in Figure 10. If the center line of draping is taken to be the origin of *y* axis, the field lines on the +*y* and −*y* will tend to travel in the direction toward the origin. Since the boundary wave phenomenon is observed in the +*y* location, the observed wave is expected to be propagating in the −*y* direction toward the origin. Based on this, the estimated width of each of the oscillations is ∼147 km. Due to the practical limitations of VEX, configuration of the complete physical structure of the surface wave is not possible.

As discussed in the previous section, to check the consistency of MV analysis results, each of the magnetic field dip-to-peak and peak-to-dip over the interval (01:47:22 to 01:48:12 UT) was divided into several segments and further analyzed using MV analysis. This has revealed that there are distinct differences between the MV parameters of some of the segments and the main transition. The results indicated that while the individual segments of the main transition showed consistent variance directions, the results from segments around the peaks or dips which correspond to magnetic barrier and ionosphere, respectively, (i.e., the start and end of the individual boundary transitions) are quite different. As seen from Figure 5b, if the thickness of the ionopause boundary is represented by the width of the color-shaded regions, then the observed different widths suggest that there is a variation in the ionopause boundary thickness. For a thick boundary crossing, if the spacecraft does not cross the ionopause perpendicularly, the inbound and outbound boundary normals might not be as parallel for a curved boundary when compared to a thinner boundary crossing. The variations of the thickness of ionopause boundary are not illustrated in Figure 7. Furthermore, there is negligible non color-shaded transition between Regions i and ii, which may imply that VEX was in neither the magnetic barrier nor the ionosphere, further agreeing with our findings that the first magnetic field oscillation dip-to-peak-to-dip is an isolated flux rope.

4.4. Embedded Flux Rope in the Boundary Wave

The results from the data analysis suggest that the flux rope is observed just inside the ionopause. This leads to a couple of outstanding questions. First, how do the analysis results of the flux rope differ to the crossings of boundary wave? The hodograms of the flux rope show a smooth 180° field rotation with finite pitch angles with respect to the axis, e.g., the angle between B_{axis} and B_{in} (77°) as well as B_{out} (54°), a characteristic that is unique to flux ropes and commonly not expected from a boundary wave. In contrast, further analysis conducted on the rest of the wave train (not shown here) shows only planar field rotations (i.e., changes in a plane with negligible pitch angles). However, there is a scenario where the characteristics of a boundary wave could resemble a flux rope. Nondraped field lines can be represented locally as an ellipse with eccentricity of infinity, e.g., Figure 10a. As they progress toward the planet, the field lines start to drape around the planet. For the case of field lines at SZA of ∼90° near the center line of the draping, the eccentricity tends toward zero with the field lines extending in −X direction. If VEX crosses this point, the eccentricity will be small and result in tightly curved field lines, e.g., Figure 10b. In this case, VEX may observe a nonplanar (three-dimensional) field rotation associated with a boundary wave that can be misinterpreted as a flux rope at the first glance. Furthermore, only the first dip-to-peak-to-dip (the flux rope) shows a potato chip-shaped hodogram, while the rest shows a mixture of randomly and linearly shaped hodograms, i.e., not a flux rope. Based on the observations of (i) smooth three-dimensional 180° field rotation as shown in hodogram in Figure 9a, (ii) finite pitch angles between B_{axis} and B_{in} as well as B_{out}, and (iii) a potato chip-shaped hodogram as shown in Figure 9b, of which are all expected characteristics of a flux rope, we then suggest that the first dip-to-peak-to-dip corresponds to a flux rope that is observed in the vicinity of the ionopause.

Second, if flux ropes are normally more frequently observed deeper in the ionosphere, why is the flux rope observed so close to the boundary wave? To begin with, the IMF is observed to drape around Venus which is evident from an abrupt change of magnetic field in the B_X direction at around 01:45:30 UT (evident from Figure 5a). Through the draping of field, B_X changes from +X to −X direction. As VEX was traveling almost along the terminator on this date, if the hemisphere in which before VEX crossed the field draping is regarded as the dawn hemisphere and the hemisphere in which after VEX crossed the field draping is regarded as the dusk hemisphere, then the observations of the flux rope as well as the boundary wave were just in the dusk hemisphere, which is only about 2 min after the center of the draping was crossed. However, the characteristics of the magnetic field in the flux rope are found to be similar to the magnetic field in the dawn hemisphere, where in particular the magnetic field in the X direction is positive while the Y and Z directions are close to zero. In contrast, the characteristics of the magnetic field for the rest of the wave train are similar to the magnetic field in the dusk hemisphere after crossing the draping (i.e., the field in X direction is consistently in the negative direction). Since the signatures of the flux rope is different from the boundary wave in the dusk hemisphere, results suggest that the flux rope may have been produced in the dawn hemisphere and transported to the dusk hemisphere, hence the flux rope is observed to be relatively close to or embedded in the boundary wave. Based on the similarity in diameter of both the flux rope and the boundary wave billows, the generation of the flux rope in the subsolar region by mass loading process is unlikely in this case.

In comparison to the conventional field draping pattern, *Masunaga et al.* [2011] presented a complicated interplanetary magnetic field configuration around Venus. This was for the case of parallel alignment between the incoming magnetic field lines and the Venus-Sun line, and it was associated with the loss of oxygen ions from the atmosphere. This configuration consisted of multiple reversals of the B_X component. One generation mechanism they proposed was the KHI. However, they noted a lack of previous studies showing Kelvin-Helmholtz waves directly at the polar ionopause. In our paper, even though the interplanetary magnetic field lines arrive at an angle of ∼30° (at the limit of the parallel alignment studied in *Masunaga et al.* [2011]), only one reversal of the B_X component is observed. This suggests a conventional draping pattern for this encounter. Further studies need to be conducted over a longer period of time to determine a more detailed understanding of this phenomenon.

5. Conclusion

We utilized the high-resolution data of ELS and MAG on board the Venus Express spacecraft to observe a rippling Venusian ionopause boundary on 26 June 2006. Results of MV analysis show VEX repeatedly crossed the ionopause boundary, which suggests that the ionopause is in a wave-like state. Further analysis over the duration where the boundary wave was observed identified a magnetic flux rope embedded just inside the

ionosphere. The different magnetic field component signature of both the flux rope and ionopause shows that the flux rope was produced in the dawn hemisphere and transported into the dusk hemisphere. We suggest that the boundary wave phenomenon is induced by the Kelvin-Helmholtz instability due to the large velocity shear in the terminator plane, where the rippling ionopause boundary is observed, as well as the perpendicular orientation between the magnetic field in the magnetic barrier and the wave normal of the boundary. The production of the flux rope in the subsolar region and subsequent transportation to the nightside are ruled out based on the similar diameters and close proximity between the flux rope and the ionopause boundary waves. The nature of atmospheric evolution of Venus has always been a subject for discussion, and research on how the solar wind interacts with Venus is crucial to better understand the evolution of the atmosphere for unmagnetized bodies. The observation of boundary wave serves as a fundamental example of a mechanism of physical atmosphere removal into the solar wind, e.g., production of atmospheric bubbles. The work from this paper contributes to experimental studies, in particular low-altitude field analysis of ionopause boundary disturbances in the terminator region. Future work will conduct a statistical survey of VEX data traveling in the terminator plane to measure the distribution of magnetic structures (flux ropes and atmospheric bubbles) to have a better image of how boundary waves develop and evolve.

References

Amerstorfer, U. V., N. V. Erkaev, D. Langmayr, and H. K. Biernat (2007), On Kelvin-Helmholtz instability due to the solar wind interaction with unmagnetized planets, *Planet. Space Sci.*, *55*(12), 1811–1816, doi:10.1016/j.pss.2007.01.015.

Arshukova, I., N. Erkaev, H. Biernat, and D. Vogl (2004), Interchange instability of the Venusian ionopause, *Adv. Space Res.*, *33*(2), 182–186, doi:10.1016/j.asr.2003.04.015.

Barabash, S., et al. (2007), The Analyser of Space Plasmas and Energetic Atoms (ASPERA-4) for the Venus Express mission, *Planet. Space Sci.*, *55*(12), 1772–1792, doi:10.1016/j.pss.2007.01.014.

Baumjohann, W., R. A. Treumann, and R. A. Treumann (1996), *Basic Space Plasma Physics*, vol. 57, World Sci., Imperial College Press, London.

Biernat, H. K., N. V. Erkaev, U. V. Amerstorfer, T. Penz, and H. I. M. Lichtenegger (2007), Solar wind flow past Venus and its implications for the occurrence of the Kelvin-Helmholtz instability, *Planet. Space Sci.*, *55*(12), 1793–1803, doi:10.1016/j.pss.2007.01.006.

Brace, L. H., R. F. Theis, W. R. Hoegy, J. H. Wolfe, J. D. Mihalov, C. T. Russell, R. C. Elphic, and A. F. Nagy (1980), The dynamic behavior of the Venus ionosphere in response to solar wind interactions, *J. Geophys. Res.*, *85*(A13), 7663–7678, doi:10.1029/JA085iA13p07663.

Brace, L. H., R. F. Theis, and W. R. Hoegy (1982), Plasma clouds above the ionopause of Venus and their implications, *Planet. Space Sci.*, *30*(1), 29–37, doi:10.1016/0032-0633(82)90069-1.

Coates, A. J., et al. (2008), Ionospheric photoelectrons at Venus: Initial observations by ASPERA-4 ELS, *Planet. Space Sci.*, *56*, 802–806, doi:10.1016/j.pss.2007.12.008.

Collinson, G., L. Wilson, D. Sibeck, N. Shane, T. Zhang, T. Moore, A. J. Coates, and S. Barabash (2012), Short large-amplitude magnetic structures (SLAMS) at Venus, *J. Geophys. Res.*, *117*, A10221, doi:10.1029/2012JA017838.

Dubinin, E., M. Fraenz, T. L. Zhang, J. Woch, Y. Wei, A. Fedorov, S. Barabash, and R. Lundin (2013), Plasma in the near Venus tail: Venus Express observations, *J. Geophys. Res. Space Physics*, *118*, 7624–7634, doi:10.1002/2013JA019164.

Elphic, R. C., and A. I. Ershkovich (1984), On the stability of the ionopause of Venus, *J. Geophys. Res.*, *89*(A2), 997–1002, doi:10.1029/JA089iA02p00997.

Elphic, R. C., and C. T. Russell (1983), Global characteristics of magnetic flux ropes in the Venus ionosphere, *J. Geophys. Res.*, *88*(A4), 2993–3003, doi:10.1029/JA088iA04p02993.

Elphic, R. C., C. T. Russell, J. A. Slavin, and L. H. Brace (1980), Observations of the dayside ionopause and ionosphere of Venus, *J. Geophys. Res.*, *85*(A13), 7679–7696, doi:10.1029/JA085iA13p07679.

Ferrari, A., S. Massaglia, and E. Trussoni (1982), Magnetohydrodynamic Kelvin-Helmholtz instabilities in astrophysics — III. Hydrodynamic flows with shear layers, *Mon. Not. R. Astron. Soc.*, *198*, 1065–1079.

Fontane, J., L. Joly, and J. N. Reinaud (2008), Fractal Kelvin-Helmholtz breakups, *Phys. Fluids*, *20*(9), 091109, doi:10.1063/1.2976423.

Futaana, Y., et al. (2008), Mars Express and Venus Express multi-point observations of geoeffective solar flare events in December 2006, *Planet. Space Sci.*, *56*, 873–880, doi:10.1016/j.pss.2007.10.014.

Hartle, R., and J. Grebowsky (1993), Light ion flow in the nightside ionosphere of Venus, *J. Geophys. Res.*, *98*(E4), 7437–7445, doi:10.1029/93JE00399.

Huba, J. D. (1981), The Kelvin-Helmholtz instability in inhomogeneous plasmas, *J. Geophys. Res.*, *86*(A5), 3653–3656, doi:10.1029/JA086iA05p03653.

Lammer, H., et al. (2006), Loss of hydrogen and oxygen from the upper atmosphere of Venus, *Planet. Space Sci.*, *54*(13–14), 1445–1456, doi:10.1016/j.pss.2006.04.022.

Lepping, R., and K. Behannon (1980), Magnetic field directional discontinuities: 1. Minimum variance errors, *J. Geophys. Res.*, *85*(A9), 4695–4703, doi:10.1029/JA085iA09p04695.

Luhmann, J. G., and C. T. Russell (1997), Venus: Magnetic field and magnetosphere, in *Encyclopedia of Planetary Science*, pp. 905–907, Encyclopedia of Earth Science, Springer, Netherlands.

Masunaga, K., Y. Futaana, M. Yamauchi, S. Barabash, T. L. Zhang, A. O. Fedorov, N. Terada, and S. Okano (2011), O^+ outflow channels around Venus controlled by directions of the interplanetary magnetic field: Observations of high energy O^+ ions around the terminator, *J. Geophys. Res.*, *116*, A09326, doi:10.1029/2011JA016705.

Pérez-de Tejada, H., M. Dryer, and O. L. Vaisberg (1977), Viscous flow in the near-Venusian plasma wake, *J. Geophys. Res.*, *82*(19), 2837–2841, doi:10.1029/JA082i019p02837.

Pope, S. A., M. A. Balikhin, T. L. Zhang, A. O. Fedorov, M. Gedalin, and S. Barabash (2009), Giant vortices lead to ion escape from Venus and re-distribution of plasma in the ionosphere, *Geophys. Res. Lett.*, *36*, L07202, doi:10.1029/2008GL036977.

Pope, S. A., T. L. Zhang, M. A. Balikhin, M. Delva, L. Hvizdos, K. Kudela, and A. P. Dimmock (2011), Exploring planetary magnetic environments using magnetically unclean spacecraft: A systems approach to VEX MAG data analysis, *Ann. Geophys.*, *29*(4), 639–647, doi:10.5194/angeo-29-639-2011.

Price, D. J. (2008), Modelling discontinuities and Kelvin-Helmholtz instabilities in SPH, *J. Comput. Phys.*, *227*(24), 10,040–10,057, doi:10.1016/j.jcp.2008.08.011.

Russell, C. T. (1990), Magnetic flux ropes in the ionosphere of Venus, in *Geophysical Monograph Series*, vol. 58, pp. 413–423, AGU, Washington, D. C., doi:10.1029/GM058p0413.

Russell, C. T., and R. C. Elphic (1979), Observation of magnetic flux ropes in the Venus ionosphere, *Nature*, *279*(5714), 616–618, doi:10.1038/279616a0.

Russell, C. T., R. C. Elphic, and J. A. Slavin (1979), Initial Pioneer Venus magnetic field results—Dayside observations, *Science*, *203*, 745–748, doi:10.1126/science.203.4382.745.

Russell, C. T., R. C. Elphic, and J. A. Slavin (1980), Limits on the possible intrinsic magnetic field of Venus, *J. Geophys. Res.*, *85*(A13), 8319–8332, doi:10.1029/JA085iA13p08319.

Russell, C. T., J. G. Luhmann, R. C. Elphic, F. L. Scarf, and L. H. Brace (1982), Magnetic field and plasma wave observations in a plasma cloud at Venus, *Geophys. Res. Lett.*, *9*(1), 45–48, doi:10.1029/GL009i001p00045.

Russell, C. T., R. N. Singh, J. G. Luhmann, R. C. Elphic, and L. H. Brace (1987), Waves on the subsolar ionopause of Venus, *Adv. Space Res.*, *7*, 115–118, doi:10.1016/0273-1177(87)90209-2.

Schwartz, S. J. (1998), Shock and discontinuity normals, Mach numbers, and related parameters, *ISSI Sci. Rep. Ser.*, *1*, 249–270.

Sibeck, D. G., R. Lopez, and E. Roelof (1991), Solar wind control of the magnetopause shape, location, and motion, *J. Geophys. Res.*, *96*(A4), 5489–5495, doi:10.1029/90JA02464.

Sonnerup, B. U. Ö., and L. J. Cahill Jr. (1968), Explorer 12 observations of the magnetopause current layer, *J. Geophys. Res.*, *73*, 1757–1770, doi:10.1029/JA073i005p01757.

Sonnerup, B. U. Ö., and M. Scheible (1998), Minimum and maximum variance analysis, *ISSI Sci. Rep. Ser.*, *1*, 185–220.

Spreiter, J. R., A. L. Summers, and A. W. Rizzi (1970), Solar wind flow past nonmagnetic planets—Venus and Mars, *Planet. Space Sci.*, *18*(9), 1281–1299, doi:10.1016/0032-0633(70)90139-X.

Stevenson, D. J. (2003), Planetary magnetic fields, *Earth Planet. Sci. Lett.*, *208*(1–2), 1–11, doi:10.1016/S0012-821X(02)01126-3.

Stevenson, D. J., T. Spohn, and G. Schubert (1983), Magnetism and thermal evolution of the terrestrial planets, *Icarus*, *54*(3), 466–489, doi:10.1016/0019-1035(83)90241-5.

Svedhem, H., D. V. Titov, F. W. Taylor, and O. Witasse (2007a), Venus as a more Earth-like planet, *Nature*, *450*(7170), 629–632, doi:10.1038/nature06432.

Svedhem, H., et al. (2007b), Venus Express—The first European mission to Venus, *Planet. Space Sci.*, *55*(12), 1636–1652, doi:10.1016/j.pss.2007.01.013.

Terada, N., S. Machida, and H. Shinagawa (2002), Global hybrid simulation of the Kelvin-Helmholtz instability at the Venus ionopause, *J. Geophys. Res.*, *107*(A12), 1471, doi:10.1029/2001JA009224.

Theis, R. F., L. H. Brace, K. H. Schatten, C. T. Russell, J. A. Slavin, and J. A. Wolfe (1981), The Venus ionosphere as an obstacle to the solar wind, *Adv. Space Res.*, *1*(1), 47–60, doi:10.1016/0273-1177(81)90087-9.

Titov, D. V., et al. (2006), Venus Express science planning, *Planet. Space Sci.*, *54*(13–14), 1279–1297, doi:10.1016/j.pss.2006.04.017.

Way, M. J., A. D. Del Genio, N. Y. Kiang, L. E. Sohl, D. H. Grinspoon, I. Aleinov, M. Kelley, and T. Clune (2016), Was Venus the first habitable world of our solar system?, *Geophys. Res. Lett.*, *43*, 8376–8383, doi:10.1002/2016GL069790.

Wei, H., C. Russell, T. Zhang, and M. Dougherty (2010), Comparison study of magnetic flux ropes in the ionospheres of Venus, Mars and Titan, *Icarus*, *206*(1), 174–181, doi:10.1016/j.icarus.2009.03.014.

Wolff, R. S., B. E. Goldstein, and C. M. Yeates (1980), The onset and development of Kelvin-Helmholtz instability at the Venus ionopause, *J. Geophys. Res.*, *85*(A13), 7697–7707, doi:10.1029/JA085iA13p07697.

Zhang, T. L., et al. (2006), Magnetic field investigation of the Venus plasma environment: Expected new results from Venus Express, *Planet. Space Sci.*, *54*, 1336–1343, doi:10.1016/j.pss.2006.04.018.

Zhang, T. L., et al. (2007), Little or no solar wind enters Venus' atmosphere at solar minimum, *Nature*, *450*(7170), 654–656, doi:10.1038/nature06026.

Zhang, T. L., et al. (2008a), Initial Venus Express magnetic field observations of the magnetic barrier at solar minimum, *Planet. Space Sci.*, *56*(6), 790–795, doi:10.1016/j.pss.2007.10.013.

Zhang, T. L., et al. (2008b), Initial Venus Express magnetic field observations of the Venus bow shock location at solar minimum, *Planet. Space Sci.*, *56*(6), 785–789, doi:10.1016/j.pss.2007.09.012.

Zhang, T. L., J. Du, Y. J. Ma, H. Lammer, W. Baumjohann, C. Wang, and C. T. Russell (2009), Disappearing induced magnetosphere at Venus: Implications for close-in exoplanets, *Geophys. Res. Lett.*, *36*, L20203, doi:10.1029/2009GL040515.

Zhang, T. L., et al. (2012), Magnetic reconnection in the near Venusian magnetotail, *Science*, *336*, 567–570, doi:10.1126/science.1217013.